Double-electron capture and population of Rydberg levels in slow Ar^{8+}+He collisions

S. Bliman,[1] M. Cornille,[2] B. A. Huber,[3] and J. F. Wyart[4]
[1]*Université de Marne-La-Vallée, 93166 Noisy-Le-Grand, France*
[2]*DARC, Observatoire de Paris, F-92195 Meudon Cedex, France*
[3]*CEA, Département de Recherche Fondamentale sur la Matière Condensée, AIM, 38054 Grenoble Cedex 9, France*
[4]*Laboratoire Aimeé Cotton, Batiment 505, Université Paris–Sud, 91405 Orsay, France*
(Received 28 May 1997)

Double-electron capture by Ar^{8+} from He is analyzed. Since the incident ion beam contains a metastable fraction of the order 5%, two distinctly behaving systems are considered: (1) $Ar^{8+}(2p^6)^1S_0 + He \rightarrow Ar^{6+}(2p^6nln'l')^{2S+1}L_J + He^{2+}$ and (2) $Ar^{8+}(2p^53s)^3P_J + He \rightarrow Ar^{6+}(2p^53snln'l')^{2S+1}L_J + He^{2+}$. For process (1), the comparison of translational energy gain and Auger spectra, with an extensive set of calculated data, supports the conclusion of an asymmetric double-electron transfer peaking at $Ar^{6+}(2p^63d4f)$ with a Rydberg tail getting to $(3lnl')$ with $n \cong 20$ $(l=1,2)$. For process (2), the double capture points dominantly into triply excited states $Ar^{6+}(2p^53s3l4l')^{2S+1}L_J$. These are above the second ionization limit of the ground state $Ar^{6+}(2p^63s^2)^1S_0$. Their decay takes place via two successive Auger steps: the first ending in the intermediate levels, $Ar^{7+}(2p^53l3l')^{2,4}L_J$. These, in turn, autoionize to the $Ar^{8+}(2p^6)^1S_0$ continuum. Both are identified in the Auger spectrum. These observations raise the question of the meaning of the auto transfer to Rydberg states and of correlated double capture processes. [S1050-2947(97)03112-0]

PACS number(s): 34.70.+e

I. INTRODUCTION

Even though much attention was given to the system Ar^{8+}+He, being studied by different experimental techniques [1], there are still some aspects not yet fully understood that are related to the double-electron capture process. It was shown, on the basis of the extended Coulomb barrier model and of the reaction window concepts [2,3] that double capture populates $(n=3, n'=3)$ and mostly $(n=3, n'=4)$, with a partial cross section ratio of 4 to 1 in favor of $(n=3, n'=4)$. This system shows the same behavior as the system O^{8+} + He for both the single and double transfer [4].

However, the problems still open relate to the analysis of minor double transfer channels, not predicted by Landau-Zener–type calculations (Rydberg level population [5], electron transfer mechanism [6], and to the problem of auto transfer to Rydberg levels [7]). A common feature of many of the reports describing double transfer is that the atomic characteristics of doubly excited populated levels were generally not well known and had scarcely been calculated. Moreover, they do not account for the sharing between autoionization and radiation mostly dependent on the total fluorescence yield of each individual level [1].

Since the Ar^{8+} ion beam contains a long-lived metastable fraction ($\sim 5\%$) [1] the question of a possible double transfer ending in triply excited states has to be addressed as well as their stabilization mechanism (radiative and/or Auger). In Sec. II, a brief outline of the experimental procedure is given. In Sec. III, an analysis of the single capture by the metastable projectile (contained in the incident ion beam and contributing to the autoionizing decay), and a review of the double capture by the ground-state projectile making use of energy levels calculations is presented in Sec. IV, the dominant double capture populated levels of the metastable projectile are identified and their stabilization is discussed.

II. EXPERIMENTAL TECHNIQUES AND RESULTS

Briefly, an Ar^{8+} ion beam (delivered by the ECR ion source in Grenoble) is passed in a collision chamber where the target gas (He) is kept at a pressure of order 4×10^{-3} Pa (measured with a Baratron). The collision chamber is differentially pumped. The beam current is typically 5 μA at 80 keV and contains a metastable fraction (in states $2p^53s\ ^3P_{0,2}$) of order 5% [1].

In order to study the double-electron-capture process

$$Ar^{8+}(2p^6)^1S_0 + He \rightarrow Ar^{6+}(2p^6nln'l')^{1,3}L_J + He^{2+} \quad (1)$$

and differentiate with process (3) hereafter, two instrumental methods are employed.

(i) The translational energy gain spectroscopy (TES): the instrument is described elsewhere [8,9]. It is used to analyze the ions of charge +6, which represent the fraction of the double capture that retained both transferred electrons and thus decayed radiatively:

$$Ar^{6+}(2p^6nln'l')^{1,3}L_J \rightarrow Ar^{6+}(2p^63s^2)^1S_0 + h\nu. \quad (2)$$

A typical energy gain spectrum of Ar^{6+} ions formed in process (1) is shown in Fig. 1. The maximum peak intensities in the energy gain distribution correspond to the population of the states $Ar^{6+}(2p^63d4d)$ and $Ar^{6+}(2p^63d4f)$ characterized by an energy gain of the order 67 eV. These states are just located below the first ionization limit in the Mg-like argon ion energy scale [10]. All contributions with energy gains less than 67 eV are associated with levels above the first ionization limit of Ar^{6+} that have shared their stabilization between photon and electron emission (Fig. 2 right side).

(ii) The Auger electron spectrometry: the instrument is fully described by Mack [14]. A typical Auger spectrum taken (at the ECR ion source in Groningen [14]) at an angle

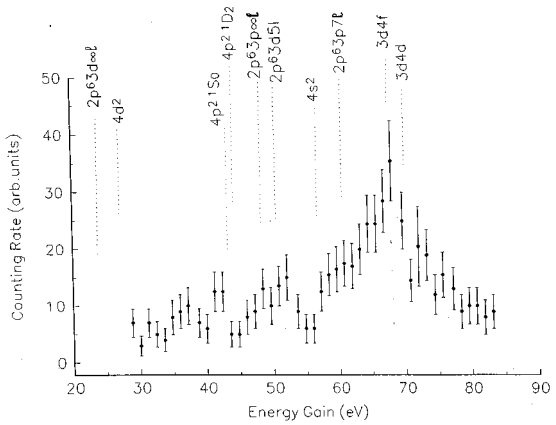

FIG. 1. TES for $Ar^{8+}(2p^6)^1S_0+He\rightarrow Ar^{6+}(2p^6nln'l')+He^+$. Ar^{6+} are detected. The energy intervals correspond to the different series likely to share their stabilization between autoionization and radiation are shown.

of 50° with respect to the ion beam incident direction is shown (Fig. 3). It extends over the energy interval 0–260 eV in the emitter frame. It contains two distinct parts: one ranging from 100 eV up to 260 eV with high intensity; the other of weaker intensity extends from 0 to 45 eV approximately. A similar spectrum was taken by Boudjema [11] at 10° from the incident ion beam and shows exactly the same features. The spectra are identical.

III. DATA ANALYSIS AND INTERPRETATION: SINGLE CAPTURE BY THE METASTABLE ION AND DOUBLE CAPTURE BY THE GROUND-STATE ION

It is well known that in the observation of charge changing ion (highly charged) atom collisions the projectile loses energy in stripping whereas it gains energy in electron capture, with zero energy gain generally setting the limit to populated levels in capture. In the following, we will separate the discussion into two parts. We first focus the attention on the Auger spectrum extending from 100 to 260 eV.

A. Single-electron capture by the metastable projectile Auger spectrum 100–260 eV

This range contains the most intense part of the Auger spectrum. It is identified as due to the stabilization of states populated by single-electron transfer to the metastable projectile according to the collision process

$$Ar^{8+}(2p^53s)^3P^o_{0,2}+He\rightarrow Ar^{7+}{**}(2p^53snl)^{2,4}L_J+He^+ \tag{3}$$

(with $n=4$ being mostly populated) followed by

$$Ar^{7+}{**}\rightarrow Ar^{8+}(2p^6)^1S_0+e, \tag{4a}$$

$$Ar^{7+}{**}\rightarrow Ar^{7+}(3s)^2S_{1/2}+h\nu. \tag{4b}$$

The most intense peaks are identified as originating from the dominantly populated levels $2p^53s4f\ ^2L_J$ (at 190 eV) and to a lesser from $2p^53s4d\ ^2L_J$ (at nearly 180 eV): these structures are identified with the aid of the calculated level energies [1].

The doublet structure at 102 eV is unambiguously attributed to the process [12] as

$$Ar^{7+}(2p^53s^2)^2P^0_{1/2,3/2}\rightarrow Ar^{8+}(2p^6)^1S_0+e. \tag{5}$$

The intermediate levels are not directly populated, as the energy gain is of the order of 125 eV, well outside the reaction window. The other lines between 100 and 180 eV are attributed to the autoionization of the $Ar^{7+}{**}(2p^53l3l')^2L_J$ levels [1] will be considered later.

Given the fluorescence yield of the levels directly populated in the single capture, there is, mostly for the quartet states, some cascade feeds to $2p^53l3l'$; these in turn would mostly radiate [12] while the doublet levels $2p^53l3l'\ ^2L_J$ mostly autoionize.

The high-energy tail extending to nearly the $2p^53s\infty l$ series limit (252 eV) is attributed to the autoionizing stabilization of high Rydberg states with n up to 10 as identified in the spectrum. The energy levels have been calculated with the assumption that for high n values, the states are nearly degenerate and that the energy values might be determined making use of the Rydberg formula (in eV)

$$E[(2p^53snl)\rightarrow(2p^6)]=252.1-13.6(8^2n^{*2}), \tag{6}$$

where n^* is the effective principal quantum number (Table I). The TES spectrum of Ar^{8+} obtained with a metastable enriched Ar^{8+} beam shows that ions that have captured one electron and then autoionize along the process

$$Ar^{7+}{**}(2p^53snl)\rightarrow Ar^{8+}(2p^6)^1S_0+e \tag{7}$$

have gained energy, which corresponds to capture into relative high n values well above $n=4$ [1].

B. Auger spectrum at 0–45 eV: TES spectrum of double capture by $Ar^{8+}(2p^6)^1S_0$

For energy gains $Q<63$ eV doubly excited levels are found above the first ionization limit of Ar^{6+}. The TES spectrum is due to double-electron capture by the ground-state $Ar^{8+}(2p^6)^1S_0$ projectiles. The part of the Auger spectrum 0–45 eV is mostly due to the double capture by the ground-state projectile except for a small part between 8 and 14 eV that we discuss below. The overall intensity variation shows a regular n^{-3}-type decrease (n principal quantum number). At the time of the experiment, few data were available for identifying levels in the Mg-like Ar^{6+} system [10,15,16,17]. Line identifications were only made up to the first ionization limit. For the purpose of identifying levels beyond this limit, two sets of calculations have been performed.

1. Calculation of the atomic parameters for $Ar^{6+}(2p^64l4l')$ and analysis

To calculate the level energies E, wavelengths λ, radiative probabilities A_r^{sf}, and the sum of all the probabilities to all lower levels $\Sigma_f A_r^{sf}$, we used the program SUPERSTRUCTURE developed by Eissner *et al.* [18]. This code is appropriate for the calculation of large quantities of atomic

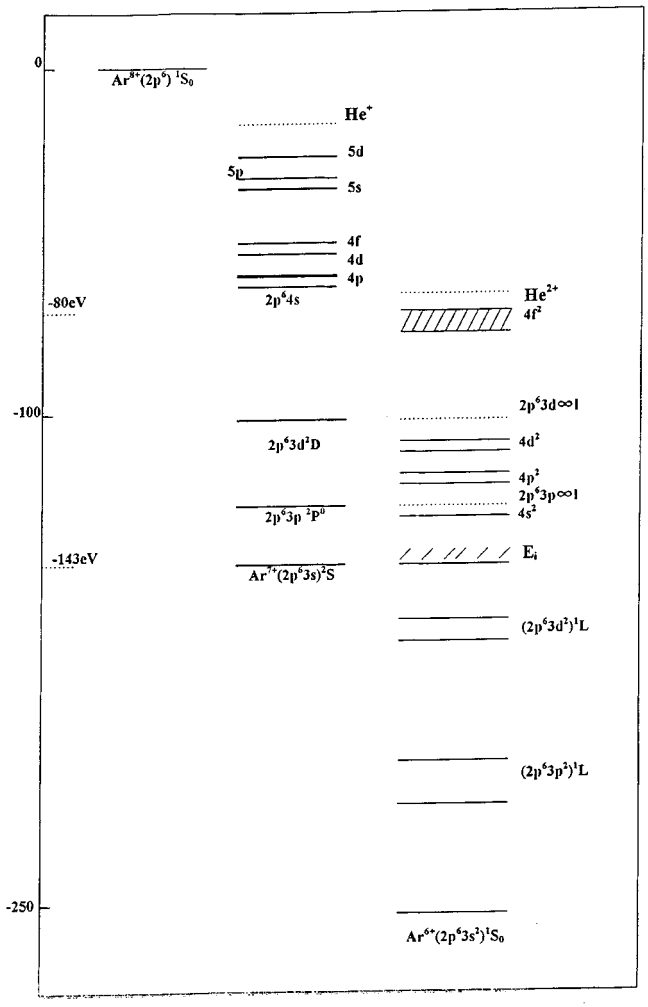

FIG. 2. Level diagram showing from the entrance channel (left side), the SC channel (central part), and the DC channel (right side); are also indicated He^+ and He^{2+} border lines between endo and exo energetic populated levels.

data as it uses a model potential, which is of the Thomas-Fermi-Dirac type. The method takes into account the average effect of repulsion of other electrons, which leads to a central potential $V(r)$, satisfying the following boundary conditions:

$$V(r)=\begin{cases} Z/r & \text{when } r\to 0 \quad (8a)\\ (Z-N+1)/r & \text{when } r\to\infty, \quad (8b)\end{cases}$$

where Z is the nucleus charge and N the number of electrons $(z=Z-N)$.

To obtain greater flexibility, a scaling parameter λ_l is introduced such that all the radial functions with the same l are calculated in the same potential and are therefore orthogonal to each other, giving

$$V(r)=V(\lambda_l,r). \quad (8c)$$

This scaling parameters λ_l can be obtained by minimizing preselected terms.

The program uses multiconfigurational wave functions to derive level energies and wavelengths. For the calculation of the atomic data for highly ionized atoms, it is necessary to take relativistic corrections into account. The semirelativistic Breit-Pauli Hamiltonian in which the relativistic corrections are treated as perturbations is convenient. This Hamiltonian is given by the following expression:

$$H=H^{\mathrm{BP}}=H^{\mathrm{NR}}+V^R, \quad (9)$$

where H^{NR} is the nonrelativistic Hamiltonian, V^R corresponds to the one-body operators (mass, Darwin, spin-orbit) and two-body operators (contact spin-spin, Darwin, orbit-orbit, spin-other orbit, mutual spin-orbit, spin-spin) of the relativistic corrections.

The development of the wave function of a level ΔJ on the multiconfiguration basis in intermediate coupling tJ, called *level*, is obtained by the diagonalization of the total Hamiltonian H^{BP}. This is expressed as

$$\psi(\Delta J,M)=\sum_t C(tJ,\Delta J)\Phi(tJ,M), \quad (10)$$

where Φ is obtained from the LS coupling wave function of the term $t=C\beta SL$ by

$$\Phi(tJ,M)=\sum_{M_LM_S} C^{LSJ}_{M_LM_SM_J}\Phi'(tM_LM_S), \quad (11)$$

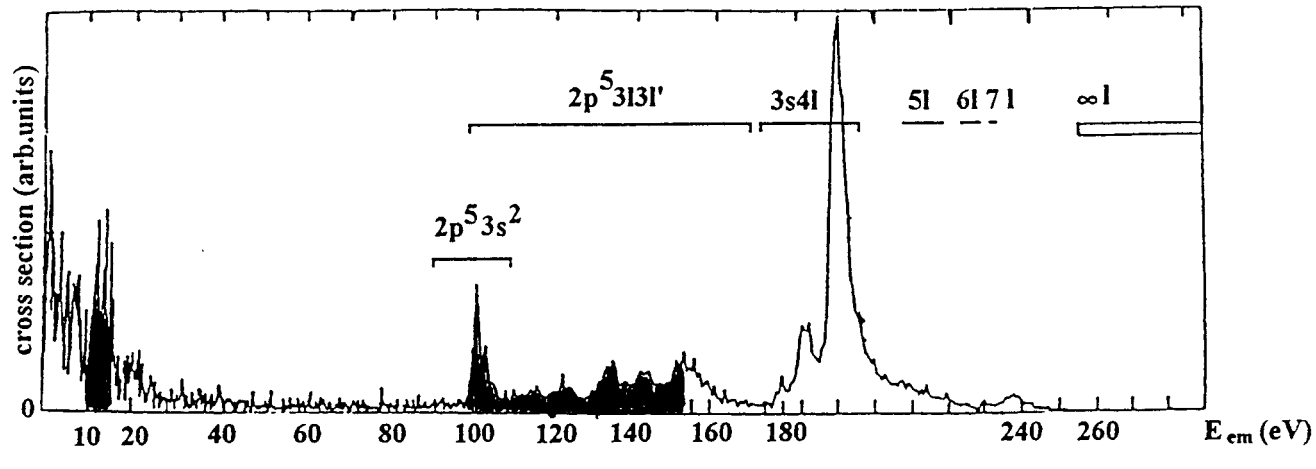

FIG. 3. Auger spectrum for Ar^{8+}+He. The regions of interest for the Auger stabilization of triply excited Ar^{6+} ions are shaded.

TABLE I. Characteristics energies of $Ar^{7+}(2p^5 3snl)$. Column 1: levels n. Column 2: energies from ground state. Column 3: energy gains. Column 4: Auger electron energies.

Levels n	Energies from GS $2p^6 3s$ (eV)	Energy gains (eV) or loss	Electron energies to $2p^6\ ^1S_0$ (eV)
5	360.8	10.3	217.3
6	371.4	−3.0	227.9
7	377.8	−6.7	234.3
8	382.0	−10.9	238.5
9	384.9	−13.8	241.4
10	386.9	−15.8	243.4
∞	395.6	−24.5	252.1

where β is a degeneracy parameter taking into account those cases where a configuration C gives rise to more than one term with the same **LS**. The coefficients $C(t\mathbf{J},\Delta\mathbf{J})$ are the *level* mixing coefficients. $C^{LSJ}_{M_L M_S M_J}$ are Clebsch-Gordan coefficients; M_L, M_S, and M_J are the projections of the momenta **L**, **S**, and **J**, respectively.

For highly ionized elements, autoionization processes are weak enough to be treated by perturbation theory. The autoionization probability A_a^{Si} is given by

$$A_a^{Si}=\frac{2\pi}{\hbar}\left|\langle\Psi_F^i(E_S)|H-E_S|\Psi_S\rangle\right|^2, \tag{12}$$

where

$$E_S=\langle\Psi_S|H|\Psi_S\rangle \tag{13}$$

and Ψ_S and Ψ_F^i are the initial *bound* state and final *free* state, respectively.

The energy E_S of the free state Ψ_F^i is taken to be the same as that of the bound state Ψ_S. The wave functions Ψ_F^i are normalized to the Dirac functions:

$$\langle\Psi_F^i(E)|\Psi_F^{i'}(E')\rangle=\delta(E-E')\,\delta_{ii'}. \tag{14}$$

The free wave function Ψ_F^i corresponds to an autoionization channel, i.e., a level ΔJ_i for the autoionized ion plus the free electron (ε,l), where ε and l are the energy and angular momentum of the free electron. As long as only large autoionization probabilities are required, the relativistic behavior of the free electron can be ignored; then the operators K and J commute with the Hamiltonian:

$$\mathbf{J_i}=\mathbf{L_i}+\mathbf{S_i},\quad \mathbf{K}=\mathbf{J_i}+l,\quad \mathbf{J}=\mathbf{K}+s, \tag{15}$$

where s is the free-electron spin ($s=1/2$).

$$A_a^{Si}=\frac{2\pi}{\hbar}\sum_{lk}\left|\sum_{tt_i}C(\Delta J_i,t_iJ_i)X(SLJ,S_iL_iJ_i,lK)\right.$$
$$\left.\times\langle t_ilJ|H-E_S|tJ\rangle C(tJ,\Delta J)\right|^2, \tag{16}$$

where $t_i=C_i\beta_i\mathbf{S_iL_i}$ is a *term* for the $(z+1)$ ion and, $\mathbf{X(SLJ,S_iL_iJ_i},l\mathbf{K})$ has been expressed by Saraph [19] as a function of the Racah recoupling coefficient W:

$$X(SLJ,S_iL_iJ_i,lK)=W(LlS_iJ_i,L_iK)W(LJS_i\ \tfrac{1}{2},SK)$$
$$\times[(2S+1)(2L+1)$$
$$\times(2K+1)(2J_i+1)]^{1/2}. \tag{17}$$

In the present work we have introduced in V^R only the one-body operators.

The calculations yield the energies of all $2p^6(4l)^2$ configurations A_a, A_{ij}, and ω_T (total fluorescence yield). From these values, the energy gains and the Auger electron energies for stabilization towards different continua are deduced. These results are shown in Table II only for singlet states. As is seen from Table II among all the $(4l4l')$ singlet levels only one $4f^2\ ^1D_2$, has a total fluorescence yield

$$\omega_T=\frac{\Sigma A_{ij}}{\Sigma A_{ij}+\Sigma A_A}, \tag{18}$$

TABLE II. Characteristics of $Ar^{6+}(2p^6 4l4l')^1L$ singlet. Column 1: levels. Column 2: energies from ground state. Column 3: total fluorescence yield (see text). Numbers in brackets represent powers of 10.

Levels	Energies (eV)	Total fluorescence yields
$1s^2 2s^2 2p^6 4s^2\ ^1S_0$	131.140 79	2.371[−06]
$1s^2 2s^2 2p^6 4s4p\ ^1P_1$	139.372 53	3.808[−05]
$1s^2 2s^2 2p^6 4p^2\ ^1D_2$	142.780 00	1.315[−05]
$1s^2 2s^2 2p^6 4p^2\ ^1S_0$	146.246 87	3.137[−05]
$1s^2 2s^2 2p^6 4s4d\ ^1D_2$	148.138 52	2.331[−04]
$1s^2 2s^2 2p^6 4s4f\ ^1F_3$	149.047 94	3.490[−06]
$1s^2 2s^2 2p^6 4p4d\ ^1D_2$	151.153 95	7.160[−05]
$1s^2 2s^2 2p^6 4p4f\ ^1F_3$	154.777 91	5.075[−04]
$1s^2 2s^2 2p^6 4p4d\ ^1P_1$	154.920 87	1.212[−05]
$1s^2 2s^2 2p^6 4p4f\ ^1G_4$	155.919 19	9.708[−06]
$1s^2 2s^2 2p^6 4p4d\ ^1F_3$	155.923 90	2.610[−05]
$1s^2 2s^2 2p^6 4p4f\ ^1D_2$	157.431 69	2.167[−05]
$1s^2 2s^2 2p^6 4d^2\ ^1D_2$	161.811 33	3.551[−02]
$1s^2 2s^2 2p^6 4d^2\ ^1G_4$	162.484 45	8.539[−06]
$1s^2 2s^2 2p^6 4d^2\ ^1S_0$	162.585 49	1.989[−06]
$1s^2 2s^2 2p^6 4d4f\ ^1F_3$	165.920 44	8.804[−06]
$1s^2 2s^2 2p^6 4f^2\ ^1G_4$	167.694 29	2.319[−06]
$1s^2 2s^2 2p^6 4d4f\ ^1P_1$	167.885 48	1.385[−05]
$1s^2 2s^2 2p^6 4f^2\ ^1D_2$	168.765 27	4.340[−01]
$1s^2 2s^2 2p^6 4f^2\ ^1S_0$	172.382 66	1.699[−04]

TABLE III. Cascade decay for $Ar^{6+}(2p^6 4f^2)\,^1D_2$; total fluorescence $\omega_T = 0.43$. Column 1: transitions. Column 2: wavelengths. Column 3: transition probabilities. Column 4: ω_{line}. Numbers in brackets represent powers of 10.

	λ (Å)	$A_i j$	ω_{line}
$1s^2 2s^2 p^6 4f^2\ ^1D_2 \rightarrow 3s4p\ ^1P_1^0$	125.06	1.080+8	2.547[−2]
$\rightarrow 3s4f\ ^1F_3^0$	140.51	1.547+8	3.649[−2]
$\rightarrow 4s4p\ ^1P_1^0$	421.82	1.322+8	3.118[−2]
$\rightarrow 4s4f\ ^1F_3^0$	628.81	1.099+8	2.592[−2]
$\rightarrow 4p4d\ ^3D_2^0$	704.01	2.831+8	6.677[−2]
$\rightarrow 4p4d\ ^3F_2^0$	707.45	6.987+7	1.648[−2]
$\rightarrow 4p4d\ ^1P_2^0$	895.56	3.600+8	8.491[−2]
$\rightarrow 4p4d\ ^1F_3^0$	965.52	9.751+7	2.299[−2]

where A_{ij} and A_a are radiative and Auger decay, respectively, ω_T is large enough to allow radiative deexcitation and decay to levels lying below it. For this level, we give, in order to appreciate the cascading effect, the most important radiative transition channels with the line fluorescence yield of each transition

$$\omega_{\text{line}} = \omega_T \times (\text{branching ratio})$$

among all these transitions (Table III), only two end levels, which in turn radiate—these are $3s4p\ ^1P_1^0$ and $3s4f\ ^1F_3^0$ both below the first ionization limit of Ar^{6+}. All other levels populated from $4f^2\ ^1D_2$ autoionize immediately. From our calculations typical lifetimes for these are in the order of 10^{-15} s. This typical decay time is of the order of the collision time

$$t_{\text{cal}} \approx \frac{\sqrt{\sigma_{\text{DC}}}}{v}, \quad \text{here } \approx 5.1 \times 10^{-16} \text{ s}, \tag{19}$$

where σ_{DC} is the total double-capture cross section (radiative and autoionization) and v the ion velocity. As seen from the transitions in Table III, it is clear that two electron-one photon transitions are possible among these discrete states in the continuum and basically have the same physical characteristics as those identified earlier among states, in Mg-like argon, below the ionization limit [14].

Table IV shows for these levels $(4l4l')$ energy gains, energies of Auger electrons decaying to the different available continua. If these were populated the electron spectrum should extend out to energies higher than 42 eV. The Auger spectrum is limited at an energy of ≅41 eV. In these conditions, we seek for further arguments to interpret this low-energy part of the spectrum.

2. Calculation of energy levels for $Ar^{6+}(2p^6 3ln'l')^{1,3}L_J$ and data analysis

A classical calculation with use of the Rydberg formula for the series $2p^6 3pnl$ and $2p^6 3dnl$ is performed. We note that terms of the series $2p^6 3pnl$ with $n \geqslant 7$ are above the first ionization limit. For the series $2p^6 3pnl$ the energies of the autoionization electron are determined from the simple relation

$$E[(2p^6 3pnl) \rightarrow (2p^6 3s)] = \Delta E[(2p^6 3p^2 P) - (2p^6 3s^2 S)] - 13.6(49/n^{*2}) \text{ eV}, \tag{20}$$

where n^* is the effective principal quantum number and $\Delta E = 17.5$ eV. The calculated energy values together with the Auger electron energies and energy gains are given in Table V for this series, where a single continuum $2p^6 3s\ ^2S_{1/2}$ is available.

For the series $2p^6 3dnl$, it is known that for $n \geqslant 5$, the levels are above the first ionization limit and for n larger seven they overlap two continua $2p^6 3s \infty l$, $2p^6 3p \infty l$. For the $(2p^6 3dnl)$ series, the electron energies are calculated according to the simple relation

$$E[(2p^6 3dnl) \rightarrow (2p^6 3s)] = \Delta E[(2p^6 3d^2 D) - (2p^6 3s^2 S)] - 13.6(49/n^{*2}) \text{ eV}, \tag{21}$$

where n^* (effective principal quantum number) and $\Delta E = 41.2$ eV, whereas the autoionization process to the $(2p^6 3p)\ ^2P^0_{1/2,3/2}$ continuum is characterized by a ΔE value of 23.7 eV. Consequently, there is a sharing with a branching ratio, which generally favors the decay to the nearest con-

TABLE IV. Energy gains and Auger electron energies for the decay to $2p^6 3s$ and $2p^6 3p$ of $Ar^{6+}[2p^6(4l)^2]\ ^1L_J$ levels. Column 1: levels. Column 2: energy from ground state (eV). Column 3: energy gains (eV). Column 4: Auger electron energies: decay to $2p^6 3s$. Column 5: Auger electron energies: decay to $2p^6 3p$.

Levels	Energies from GS ($3s^2$)	Energies gains (eV)	Autoionized energies to $2p^6 3s$	Autoionized energies to $2p^6 3p$
$2p^6 4s^2\ ^1S_0$	131.14	40.90	23.1	17.5
$2p^6 4p^2\ ^1S_0$	146.20	25.84	37.0	16.8
$2p^6 4p^2\ ^1D_2$	142.78	29.26	36.3	15.5
$2p^6 4d^2\ ^1S_0$	162.58	9.46	54.0	17.6
$2p^6 4d^2\ ^1D_2$	161.80	10.24	52.5	17.7
$2p^6 4d^2\ ^1G_4$	161.48	10.56	52.9	17.5
$2p^6 4f^2\ ^1S_0$	172.38	−0.34	63.8	17.7
$2p^6 4f^2\ ^1D_2$	168.76	3.28	59.8	17.7
$2p^6 4f^2\ ^1G_4$	167.69	4.35	59.5	17.8

TABLE V. Characteristic energies of $Ar^{6+}(2p^6 3pnl)$ Column 1: levels. Column 2: energies from ground state. Column 3: energy gains. Column 4: Auger electron energy for decay to $2p^6 3s$.

Levels n	Energies from GS $3s^2$ (eV)	Energies gain (eV)	Electron energies for decay to $3s$ (eV)
7	128.2	59.5	3.9
8	131.4	56.3	7.1
9	133.6	54.0	9.4
10	135.1	52.6	10.8
11	136.3	51.4	12.0
12	137.2	50.5	12.9
13	137.9	49.8	13.6
14	138.4	49.3	14.1
15	138.8	48.9	14.5
20	140.1	47.6	15.8
∞	141.8	45.9	17.5

tinuum. Table VI summarizes the theoretical predictions for the level energies, the energy gains, and the Auger electron energies for the decay to each available continuum. The intervals covered by each series as well as the energy gains associated with the $2p^6(4s)^2$ and $2p^6(4p)^2$ states are shown in Fig. 1 on the energy gain scale. In Fig. 4, the $3pnl$ and $3dnl$ limits for the decay to the different continua are indicated on the magnified low-energy part of the Auger spectrum, no line is attributable to $2p^6(4l)^2$. However, since the decay of line intensity in the Rydberg series is expected to be regular with a n^{-3} variation (n principal quantum number) and terminate at nearly 41 eV, we have to analyze the intensity increase of the lines in the interval 8–14 eV, which departs from the regular decay pattern.

IV. DOUBLE TRANSFER TO THE METASTABLE ION AND STABILIZATION

Since the metastable fraction content in the incident beam is of order 5% if double capture takes place the mostly populated levels are likely to be seen and thus we consider the process

$$Ar^{8+*}(2p^5 3s)\ {}^3P^0_{1,2} + He \rightarrow Ar^{6+***}[(2p^5 3s)\ {}^3P 3l4l']^{2S+1}L_J + He^{2+}. \quad (22)$$

Since the collisional features for single capture are the same for the ground state and metastable projectiles (same most populated level $n=4$ and energy gains in the exit channel), we assume that the collisional features for the double transfer are the same for both projectiles (same $nln'l'$ for the most populated levels and same energy gain). With the fact that the energy gain observed for the most populated levels in the ground-state projectile is of order ($\sim$65–67 eV), we place in the energy scale of Ar^{6+}, the levels $2p^5 3s3d4d$ and $2p^5 3s3d4f$.

They appear to be at nearly 375 eV above the ground state $Ar^{6+}(3s^2)^1S_0$.

A. Structure of the four-open-shell configuration

Ab initio studies of selected configurations of Ar^{6+} with four open shells $2p^5 3s3l4l'$ were performed, the choice for l and l' being guided by the experimental scaling law proposed by Hutton [13]. The relativistic Hartree exchange po-

TABLE VI. Characteristic energies for $Ar^{6+}(2p^6 3dnl)$ (see caption Table IV).

Levels n	Energies from GS (eV)	Energies gains (eV)	Electron energies for decay to $3s$	Electron energies for decay to $3p$
5	138.8	48.9	14.5	
6	147.0	40.7	22.7	5.2
7	151.9	35.8	27.6	10.1
8	155.1	32.6	30.8	13.3
9	157.3	30.4	33.0	15.5
10	158.8	28.9	34.5	17.0
11	160.0	27.7	35.7	18.2
12	160.9	26.8	36.6	19.1
13	161.6	26.2	37.3	19.8
14	162.1	25.7	37.8	20.3
15	162.5	25.3	38.2	21.0
20	163.8	24.0	39.5	22.3
∞	165.5	22.2	41.2	24.7

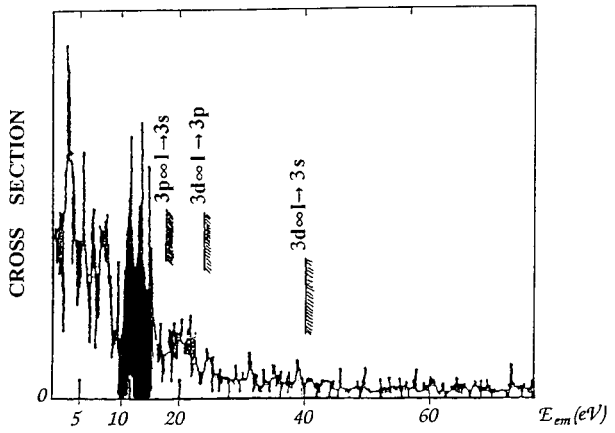

FIG. 4. Auger spectrum for the energy range 0–45 eV in the emitter frame. The region of interest for the first Auger electron emission of triply excited Ar^{6+} ions is shaded.

tential (HXR) method and the computed codes by Cowan were applied to $2p^5 3s 3d 4d$ and $2p^5 3s 3d 4f$. Due to the fact that any $3s3d$ configuration is nearly degenerate with $3p^2$, resulting in a strong mixing of their ^1D terms, it may be expected that $2p^5 3s 3d nl$ and $2p^5 3p^2 nl$ form a mixed group whatever nl is. Therefore several studies were made: (a) in the unrealistic assumption of an ''isolated'' configuration $2p^5 3s 3p 4d$ and (b) for the group $2p^5 3s 3p 3d + 2p^5 3p^2 4d$.

Although it is closer to LS than to jj coupling conditions, case (a) shows that due to the spin-orbit interaction of $2p^5$, S and L quantum numbers are inappropriate. Except for some quintet levels, intermediate coupling conditions prevail. The case (b) shows that the overlap of both configurations is about 70% of their total width and the $3s3d$-$3p^2$ interaction leads to shifts as large as 2.5 eV for some of the 350 calculated levels. The levels with dominant $2p^5 3s 3d 4d$ character are located in the range 359.6–374 eV above the ground state $3s^2\ ^1S_0$. In the case of the $2p^5 3s 3d 4f$ configuration the upper calculated level is 381 eV above the ground $3s^2$. These results are sketched in Fig. 5.

B. Stabilization of triply excited Ar^{6+} ion

Given the level energies relative to Ar^{7+} ion levels, Auger decay should involve two steps. (i) In a first step, one Auger electron is emitted,

$$Ar^{6+}(2p^5 3s 3d 4l)^{2S+1}L_J \rightarrow Ar^{7+}(2p^5 3l 3l')^2 L_J + e, \tag{23}$$

where the electron is of low energy.

(ii) Then a second Auger autoionization step would follow,

$$Ar^{7+}(2p^5 3l 3l')^2 L_J \rightarrow Ar^{8+}(2p^6)^1 S_0 + e, \tag{24}$$

where the electron has an energy of the order of 100 eV or slightly more (102–150 eV) (Fig. 3).

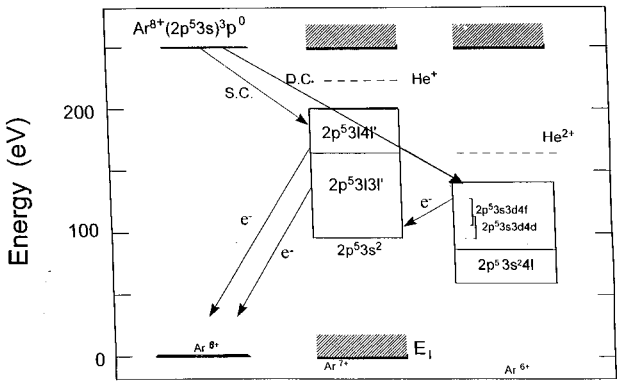

FIG. 5. Level diagram showing from the entrance channel (left side) $Ar^{8+}(2p^5 3s)^3 p^0$, the SC channel (central part) with levels $2p^5 3l 3l'$ and $2p^5 3l 4l'$ and the DC exit channels $2p^5 3s 3d 4d$ and $2p^5 3s 3d 4f$. (SC denotes single capture and DC denotes double capture.) Levels are shown above the first ionization limit of $Ar^{7+}(E_i = 143.4$ eV) central part and the second ionization limit of Ar^{6+} (sum of $E_i = 267.7$ eV) (right side).

C. Analysis of the experimental data

The likeliness of this two-step stabilization scheme is supported by two features seen in the Auger spectrum (Figs. 3 and 4).

In the low-energy part $0 < E < 40$ eV between 8 and 14 eV, a series of closely packed transitions—whose intensities are departing from a regular Rydgerg series with intensities varying as n^{-3}—are seen superimposed over the peaks due to the autoionization decay of the levels populated by double transfer to the ground-state projectile that populated $3pnl$ and $3dn'l$ states with $n \geqslant 7$ and $n' \geqslant 5$, respectively. Owing to the levels' position $2p^5 3s 3d 4d$ and $2p^5 3s 3d 4f$ relative to the levels $2p^5 3l 3l'$, these transitions are energetically possible (Fig. 5). Once the first Auger electron has been emitted, the second step ends in the release of an electron of energy between 102 and 150 eV. Some radiative cascade feed to $2p^5 3l 3l'$ comes from the single-capture levels $2p^5 3s 4d$, $4f$, dominantly quartet states, while doublets decay via an Auger process. This combined population cascade and Auger ending in $2p^5 3l 3l'$ should explain the weak lines in the energy range 102–150 eV. These levels are the intermediate continua for the first Auger step while $(2p^6)\ ^1S_0$ is the single available continuum for the Auger decay of $2p^5 3l 3l'$.

V. DISCUSSION AND CONCLUSION

Although a comparison turns out to be rather complicated, the calculated electron energies are compared with Auger energies in Table VII, for the decay of the states populated in double capture by the ground-state projectile. In the energy range 8–14 eV are seen in the superimposed closed box the electrons from the first Auger decay step of states $2p^5 3s 3d 4d$ and $4f$ to $2p^5 3l 3l'$.

From the analysis of the spectra, we have clear evidence that levels with high n values (up to $n = 20$) are populated in the symmetric Rydberg series $2p^6 3pnl$ and $2p^6 3dnl$. The $3dnl$ terms have branching ratios that favor the decay to

TABLE VII. Comparison of experimental and calculated electron energies. The box encloses the energy rfegion corresponding to the first Auger electron emitted further to the dominant double capture by the metastable projectile $Ar^{8+}(2p^5 3s)^3P^0$ into $Ar^{6+}[2p^5 3s 3d 4d$ and $3d4f]^{2S+1}$.

	Calculated $2p^6 3pnl$		Calculated $2p^6 3dnl$ energies for decay to				Calculated $2p^6(4l)^2$ energies for decay to	
			$3s$		$3p$			
Experimental	$E(n)$	n	$E(n)$	n	$E(n)$	n	$3s$ $E(n)$	$3p$ $E(n)$
3.6	3.9	7						
5.8					5.2	6		$5.6(4s^2)\ ^1S_0$
7.2	7.1	8						
9.5	9.3	9						
			27.6	7				
13.0	12.9	12						
13.2					13.3	8		
13.7	13.6	13						
	14.1	14						
14.7	14.5	15	14.5	5				
14.8								
15.8	15.8	20			15.5	9		
20.0					20.3	14		$20.2(4p^2)^1S_0$
								$20.8(4p^2)^1D_2$
23.0					22.3	20	$23.1(4s^2)^1S_0$	

$2p^6 3p$. For emission energy >25 eV, the lines for the decay to $2p^6 3s$ have extremely weak intensities. The terms $2p^6(4l)^2$ if present at all, would be limited to the decay $2p^6 4s^2$ and $2p^6 4p^2$. In the vacuum ultraviolet range no transition attributable to the optical decay of $Ar^{6+}(4f^2)\ ^1D_2$ could be seen. However, due to the configuration interaction and mixing, these terms may well couple and mix to the $3dnl$ or/and $3pnl$ terms. The terms $2p^6 3pnl$ (with $n=10$ and 11) are missing in the Auger spectrum; they (Table VII) have probably a high fluorescence yield since in the TES spectrum, a relative increase of the counting rate is measured at 52–53 eV (Fig. 1 and Table IV). The reason for this is that the overlap of the wave functions of the two electrons for significantly different n and different l is so small that the two-electron state is likely to decay radiatively and in particular for the states with the highest J values. The nonsymmetric double capture, leading dominantly to the population of $Ar^{6+}(2p^6 3d4l)^{2s+1}L_J$ and $Ar^{6+}(2p^5 3s 3d4l)^{2s+1}L_J$ states produces with small probability asymmetric Rydberg states.

Our results rather explain and support a two-step two-electron transfer mechanism to both ground- and metastable-state projectiles; coupling between symmetric $(4l4l')$ states (so far not observed) and asymmetric $(3ln'l')$ states might be effective for states of the same parity J quantum numbers and are energetically close.

For the double transfer to the metastable projectile a two Auger step stabilization process has been identified. Once the first electron of low energy is emitted the ion reaches the intermediate available continuum $[(2p^5 3l3l')^2L_J$ states] and then the second Auger electron is emitted (energies of order 102–150 eV), leaving the ion state $Ar^{8+}(2p^6)^1S_0$ [20–22]. The auto transfer to Rydberg state (ATR) mechanism [23,24] for populating asymmetric Rydberg states cannot be identified in the present results.

[1] S. Bliman, M. G. Suraud, D. Hitz, B. A. Huber, H. Lebius, M. Cornille, J. E. Rubensson, J. Nordgren, and E. J. Knystautas, Phys. Rev. A **46**, 1321 (1992).

[2] A. J. Niehauss, J. Phys. B **19**, 2925 (1986).

[3] A. Barany, G. Astner, H. Cederquist, M. Danared, S. Huldt, P. Hvelplund, A. Johnson, H. Knussen, L. Lilejby, and K. G. Rensfeldt, Nucl. Instrum. Methods Phys. Res. A **39**, 397 (1985).

[4] S. Bliman, D. Hitz, B. Jacquot, C. Harel, and A. Salin, J. Phys. B **16**, 2849 (1983).

[5] S. Bliman, J. Nordgren, E. J. Knystautas, and M. G. Suraud, J. Phys. B **25**, L135 (1992).

[6] N. Stolterfotht, C. C. Havener, R. A. Phaneuf, J. K. Swenson, S. M. Shafroth, and F. W. Meyer, Phys. Rev. Lett. **57**, 74 (1986).

[7] P. Roncin, M. N. Gaboriaud, M. Barat, Montesquieu A. Bordenave, P. Moretto-Capelle, M. Benhenni, H. Bachau, and C. Harel, J. Phys. B **26**, 4181 (1993).

[8] B. A. Huber, Comments At. Mol. Phys. **21**, 15 (1987).

[9] H. Lebius and B. A. Huber, Z. Phys. D **21**, S271 (1991).

[10] P. Marseille, S. Bliman, P. Indelicato, and D. Hitz, J. Phys. B **20**, L423 (1987).
[11] M. Boudjema, Ph.D. thesis, Université d'Alger, Algeria, 1990 (unpublished).
[12] S. Bliman, M. G. Suraud, D. Hitz, J. E. Rubensson, J. Nordgren, M. Cornille, P. Indelicato, and E. J. Knystautas, J. Phys. B **22**, 3647 (1989).
[13] R. Hutton, M. H. Prior, S. Chantrenne, M. H. Chen, and D. Schneider, Phys. Rev. A **39**, 4902 (1989).
[14] E. M. Mack, Ph.D. thesis, University of Utrecht, The Netherlands (1987).
[15] S. Bliman and M. Cornille, Nucl. Instrum. Methods Phys. Res. B **87**, 51 (1994).
[16] P. Marseille, S. Bliman, J. P. Desclaux, S. Dousson, and D. Hitz, J. Phys. B **20**, 5127 (1987).
[17] S. Bliman, P. Indelicato, D. Hitz, P. Marseille, and J. P. Desclaux, J. Phys. B **22**, 2741 (1989).
[18] W. Eissner, N. Jones, and H. Nussbaumer, Comput. Phys. Commun. **8**, 270 (1974).
[19] H. E. Saraph, Comput. Phys. Commun. **3**, 256 (1972).
[20] R. D. Cowan, *The Theory of Atomic Structure and Spectra* (University of California Press, Berkeley, 1981), and computer codes.
[21] M. R. Flannery, in *Atomic, Molecular, Optical Physics*, edited by G. W. Drake (AIP Publications, New York, 1996), Chap. 43, p. 505.
[22] S. Bliman, R. Bruch, P. L. Altick, D. Schneider, M. H. Prior, Phys. Rev. A **53**, 4176 (1996).
[23] H. Bachau, P. Roncin, and C. Harel, J. Phys. B **25**, L109 (1992).
[24] H. Bachau, C. Harel, M. Barat, P. Roncin, A. Bordenave-Montesquieu, P. Moretto-Capelle, X. Benoit-Cattin, A. Gleizes, and M. Benhenni, in *VIth International Conference on the Physics of Highly Charged Ions*, edited by P. Richard, M. Stockli, C. L. Cocke, and C. D. Lin, AIP Conf. Proc. No. 274 (AIP, New York, 1993).